JOURNAL OF SOLID STATE CHEMISTRY 29, 63–72 (1979)

Absorption and Emission Spectroscopy and Magnetic Susceptibility of Sodium β-Alumina Doped with Mn, Co, and Ni

JAMES R. AKRIDGE AND JOHN H. KENNEDY*

Department of Chemistry, University of California, Santa Barbara, California 93106

Received May 11, 1978; in revised form September 14, 1978

The absorption spectrum and magnetic susceptibility vs temperature have been measured for β-alumina doped with Mn, Co, and Ni. In addition, the emission spectra of Mn-doped samples have been measured. Mn and Co are shown to occupy tetrahedral sites and to be in the +2 oxidation state in β-alumina, in agreement with the results of previous investigators. Nickel is shown to occupy both octahedral and tetrahedral sites in β-alumina. Evidence indicates that nickel on octahedral sites is in the +3 oxidation state while that occupying tetrahedral symmetry sites is in the +2 oxidation state. The bands in the absorption spectrum for each metal are assigned and Dq, B, and C are calculated where possible.

Introduction

It is well known that addition of M^{2+} ions to β-alumina increases the ionic conductivity of sodium β-alumina. Location of the impurity dopant in the β-alumina lattice has not always been determined and this, along with confirmation of the oxidation state of the metal dopant following sintering, would be useful information for understanding the role of the dopant in modifying β-alumina properties.

Normal sintering conditions for β-alumina are at temperatures of about 1600°C for 2–3 hr in an air atmosphere. These high-temperature conditions could lead to changes in the oxidation states of metal dopants. This could result in some unexpected results when the conductivity and other properties of M^{2+}-doped β-aluminas are investigated. In fact, we have reported (*1*, *2*) that oxidation-state changes from the initial presintered metal-doped β-alumina do occur with Fe and Cr.

Experimental

Procedures for doping with metal nitrates as starting materials, firing, and measuring absorption and emission spectra and magnetic susceptibilities have been published previously (*1*). In the present study MnO_2 was also used as a dopant to determine if Mn^{4+} could be stabilized in β-alumina.

Samples of each metal-doped β-alumina were hot pressed using graphite dies. Only cobalt-doped β-aluminas could be successfully hot pressed in direct contact with graphite, manganese and nickel being reduced to the metals. A manganese sample was successfully hot pressed without reduction to the metal at the center 50% of a disk 1.2 cm in diameter, by protection from direct contact with the graphite rams using spacers of tantalum metal 0.05 cm thick. The tantalum stuck to the hot-pressed disk

* Author to whom correspondence should be addressed.

0022-4596/79/070063-10$02.00/0

surfaces and had to be ground off with 300-mesh SiC. The resulting manganese hot-pressed disk was light green. Nickel could not be hot pressed without complete reduction to the metal even when protected from direct contact with graphite.

The hot-pressed manganese sample was used to record a room temperature spectrum after lapping it to 0.1 mm thickness. The sample was sufficiently transmitting to enable it to be placed directly into the sample compartment of a Cary 15 UV-Visible spectrophotometer. This same procedure was followed for a 1 w/o doped nickel sample following air sintering. The 0.1-mm thickness allowed the Cary 15 to be used. Spectra at liquid nitrogen temperature were recorded photographically (*1*). Additionally, each doped material was heated for 5 hr at 1200°C in a flowing stream of 10% H_2/90% N_2 to determine the effect of a reducing atmosphere. No change was noted for manganese and cobalt. Nickel was reduced to the free metal by firing in the reducing atmosphere.

β-Aluminas to be analyzed were dissolved in boiling concentrated phosphoric acid. Similarly, aqueous metal standards were also boiled with an equal quantity of concentrated phosphoric acid. However, β-alumina samples were <200 mg since samples >200 mg were not readily dissolved in a 10-ml portion of concentrated phosphoric acid. Fine powders were necessary and very thorough boiling in acid was essential. A fully dissolved sample resulted in a clear (color depending upon metal dopant) phosphoric acid solution which gelled upon cooling to room temperature. Following sample dissolution the appropriate spectrophotometric procedure (*3*) was followed for the metal involved. A Bausch & Lomb Spectronic 20 was used to read absorption following color development.

A second analysis was performed by Laboratoire d'Analyses de Recherches et d' Essais Chimiques, E.N.S.E.E.G. Service Larec, Domaine Universitaire, 38401 Saint Martin D'Heres, France, using atomic absorption spectroscopy. The results of this second analysis were in full agreement with the colorimetric analysis.

Manganese

Absorption Spectrum

The absorption spectrum of manganese in β-alumina host lattice was invariant with firing atmosphere. Figure 1 shows the absorption bands obtained at 77°K. Since previous work had strongly indicated that the Mn^{2+} ion was present in tetrahedral coordination in β-alumina hosts from luminescence (*4, 5*) and ESR (*6, 7*) investigations, it was assumed that the absorption bands were from tetrahedral Mn^{2+} for making a trial assignment of the bands.

The absorptions $^4A_1, ^4E(^4G) \leftarrow {}^6A_1(^6S)$ and $^4E(^4D) \leftarrow {}^6A_1(^6S)$ are independent of

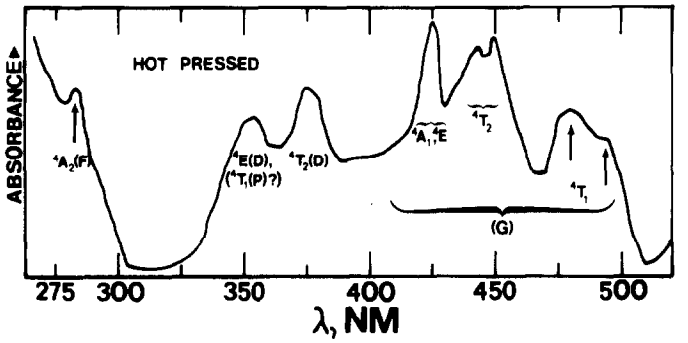

FIG. 1. Absorption spectrum at 77°K of 4 w/o Mn-doped β-alumina; hot-pressed sample.

the crystal-field strength and are of the same subshell configuration, $e^2t_2^3$. It can be expected that these bands should be narrow and temperature independent. The absorptions at 23 530 cm^{-1} (425 nm) and 27,930 cm^{-1} (358 nm) changed least when spectra at 300 and 77°K were compared. They were, therefore, assigned to the transitions stated above. The energy relationships for these bands have been calculated by Tanabe and Sugano (*8*). The Racah parameters B and C were calculated and with these values and the Tanabe–Sugano interaction matrices for $^4T_1(^4G)$ and $^4T_2(^4G)$, assigned to the first and second lowest observed energy absorptions, respectively, a "best-fit" value of Dq was calculated. Results are contained in Table I. The results are in very close agreement with those obtained with Mn-doped $MgGa_2O_4$ (*9*), where Mn^{2+} is present in tetrahedral coordination.

The absorption spectrum (Fig. 1) shows that the degeneracy of the $^4T_1(^4G) \leftarrow {}^6A_1(^6S)$ and $^4T_2(^4G) \leftarrow {}^6A_1(^6S)$ absorptions are lifted, although the band splitting could only be seen at 77°K. The lifting of the degeneracy of those absorptions is as expected since the site symmetry of the Al(2) and Al(3) four-coordinate sites in the β-alumina spinel block are at best C_{3v} (*10*). The maximum degeneracy allowed in C_{3v} symmetry is twofold. The splitting of the $^4T_2(^4D)$ could not be detected probably because of insufficient resolution. Studies of Mn^{2+} in lower-symmetry hosts (*11*) have shown that the splitting of the $^4T_2(^4D)$ is rather small compared to that for the $^4T_1(^4G)$ and $^4T_2(^4G)$.

Emission Spectrum

The emission spectrum of manganese in β-alumina is shown in Fig. 2. The emission is

TABLE I

EXPERIMENTAL AND CALCULATED ABSORPTION BAND POSITIONS AND BAND ASSIGNMENTS FOR METAL-DOPED β-ALUMINAS

Metal	Firing atmosphere	Host lattice	Band positions (experimental)[a]	Assignment	Band positions (calculated)	Dq	B	C
Mn	N_2/O_2 or H_2/N_2	β-Al_2O_3	T_d: 20 270	$^4T_1(G) \leftarrow {}^6A_1(S)$	20 500	520	630	3 450
			22 370	$^4T_2(G) \leftarrow$	22 600			
			23 530	$^4A_1, {}^4E(G) \leftarrow$	23 550			
			26 310	$^4T_2(D) \leftarrow$	26 800			
			27 930	$^4E(D), (^4T_1(P)?) \leftarrow$	27 960			
			36 360	$^4A_2(F) \leftarrow$	38 310			
Co	N_2/O_2 or H_2/N_2	β-Al_2O_3	T_d: 16 130					
			17 240	$^4T_1(P) \leftarrow {}^4A_2(F)$				
			18 080					
			20 890	$^2A_1(G) \leftarrow$				
			24 440	$^2T_2(G) \leftarrow$				
Ni	N_2/O_2	β-Al_2O_3	T_d: 3 000	$^3T_2(F) \leftarrow {}^3T_1(F)$	2 880	344	860	—
			15 430					
			16 530	$^3T_1(P) \leftarrow$	15 215			
			—	$^3A_2(F) \leftarrow$	6 318			
			O_h: 20 414	$^4T_{2g}(F) \leftarrow {}^4T_{1g}(F)$	20 770	2 262	1 077	—
			34 480	$^4T_{1g}(P) \leftarrow$	35 156			
			—	$^4A_{2g}(F) \leftarrow$	43 080			

[a] Error is ±100 cm^{-1}.

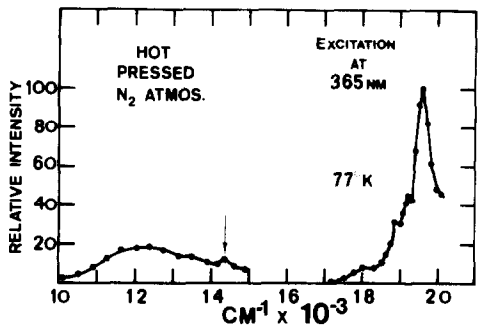

FIG. 2. Emission spectrum of Mn-doped β-alumina. Sample of Fig. 1.

composed of a very strong emerald-green band and a weaker band in the near ir. The green emission is assigned to the $^6A_1(^6S) \leftarrow {}^4T_1(^4G)$ phosphorescence. This assignment is in agreement with other investigations (*9*). The green emission is composed of more than one band which results from the lifting of the $^4T_1$ degeneracy by the lower-than-tetrahedral site symmetry. The position of the green emission is in very close agreement with the center of the $^4T_1(^4G)$ absorption. Such a small Stokes shift would indicate that the average internuclear separation between the $^6A_1(^6S)$ ground state and the $^4T_1(^4G)$ excited state is about equal. The green emission is very similar to that of $ZnAl_2O_4$ (*9, 12*), $MgAl_2O_4$ (*12*), $MgGa_2O_4$ (*9*), and β-$LiAl_5O_8$ (*13*) which all have Mn^{2+} on tetrahedral sites. The green phosphorescence band in β-alumina is concluded to be Mn^{2+} in tetrahedral site symmetry.

The band in the near ir could result from several possibilities. Examination of the Tanabe–Sugano diagram shows that the $^4T_1(^4G)$ state decreases in energy relative to the ground state as Dq increases. If Mn^{2+} were present in one of the two sixfold coordination sites (*10*) existing in β-alumina the emission could be expected in the far red or near ir as observed. However, the fact that Boilot *et al.* (*14*) observed no EPR signal which could be attributed to hexacoordinate Mn(II) in the spinel block makes assignment of the red band to hexacoordinate Mn(II) unjustified. Mn(IV) emits in the region of $14\,000^{-1}$–$17\,000\ cm^{-1}$ (*4, 13*), but since the observed emission was the same for both reducing and oxidizing conditions, Mn(IV) was probably not responsible. Emission from Mn(II) on sodium sites (Beevers–Ross sites) has been reported to occur at higher energy ($16\,950\ cm^{-1}$) (*4*) and so the red band could not be attributed to that sixfold coordinate position even though some Mn(II) may occupy that site (*4, 14*). Hence, the band does not appear to be due to manganese and an impurity source may be responsible. It should be noted that iron(II), normally present as an impurity in β-alumina, does emit in the region of the red band (*1*). Therefore we conclude that the emission is most likely the result of an iron impurity.

The absorption and emission spectra presented here both support the assignment of tetrahedral coordination for Mn(II) in β-alumina. Boilot *et al.* (*14*) have assigned Mn(II) to the 4*f* [Al(2)] (*10*) site in β-alumina as well as to the BR (Beevers–Ross site) sodium site in the conducting plane (after ion exchange in molten $MnCl_2$) using EPR spectroscopy. The prior study by Bergstein and White (*4*) of the emission of Mn(II) in β-alumina resulted in conclusions identical to those of Boilot *et al.* (*14*) except for the exact lattice site for Mn(II) in the spinel block of β-alumina. The more recent study (*5*) of Mn(II) emission in the β-aluminas also shows fourfold coordination for Mn(II). Antoine (*15*) recorded absorption spectra for Mn(II) in single-crystal β-alumina obtained by rf melting of appropriate mixtures of sodium carbonate, aluminum oxide, and MnO_2. His results are in full agreement with those presented in this report except for the observation of the lifting of the degeneracy of the $^4T_1(^4G)$ and $^4T_2(^4G)$ absorptions which were not observed in his spectra taken at room temperature.

Magnetic Susceptibility

Figure 3 shows the behavior of χ_M^{-1} vs T. As expected for a d^5 high-spin system where

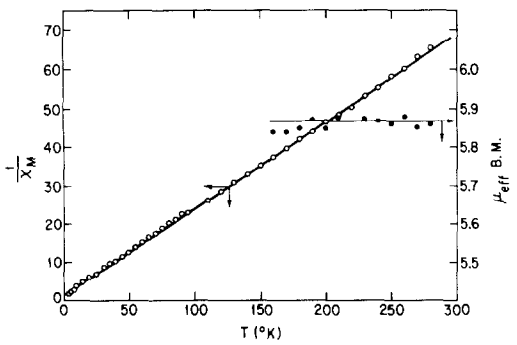

FIG. 3. Temperature dependence of the magnetic susceptibility and magnetic moment for Mn-doped β-alumina.

spin–orbit coupling effects and contributions from the second-order Zeeman effect are absent, linear behavior was displayed. Mn(II) obeys the simple Curie–Weiss law. The magnetic moment calculated from the slope of Fig. 3 is 5.87 ± 0.02 Bohr magnetons (μB), in excellent agreement with the spin-only moment of 5.92 μB expected for ideal behavior. The magnetic behavior fully supports the contention that the Mn(II) ion is high spin in β-alumina. (The Weiss temperature of Fig. 3 is 3.3 ± 3°K which makes it zero for all practical purposes.) An estimate of temperature-independent paramagnetism (TIP) can be made from a plot of χ_M vs $(T-\theta)^{-1}$ and is $2.5\times10^{-4}\pm1.3\times10^{-4}$ erg/G^2 mole. This very small TIP or second-order Zeeman effect contribution is insignificant compared to the χ_M of 1.5×10^{-2} erg/G^2 mole at 280°K.

The linearity of Fig. 3 also shows that if Mn(IV) were present it was at a concentration too low to affect the magnetic behavior. This is because Mn(IV) on a tetrahedral site would have a $^4T_1$ ground state, and $3d$ ions with "T" ground-state symmetry have magnetic moments which are temperature dependent. On the other hand, if Mn(IV) were present on an octahedral site the χ_M^{-1} vs T plot would display Curie law-type behavior but the magnetic moment would be lower than the d^5 spin-only value.

Cobalt

Absorption Spectrum

It is known from the X-ray study of Dernier and Remeika (*16*) that Co(II) is present in tetrahedral coordination in β-alumina and resides on the Al(2) site in the center of the spinel block. The $^4T_1(^4P) \leftarrow {}^4A_2(^4F)$ transition (Fig. 4) is split into a triplet which is often observed for

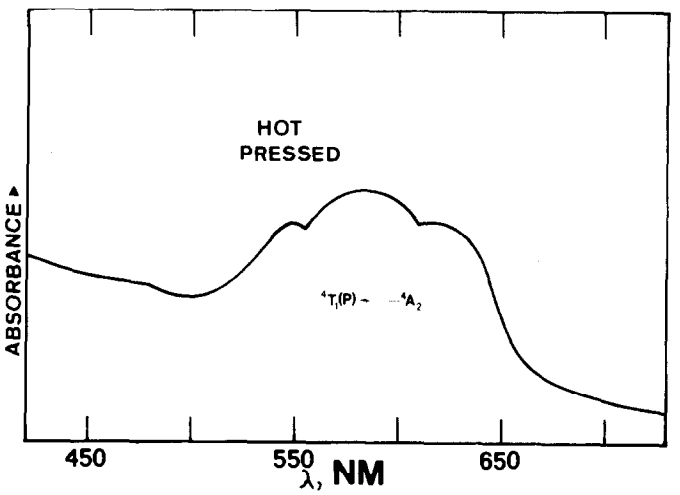

FIG. 4. Absorption spectrum at 77°K of 0.1 w/o Co-doped β-alumina; hot-pressed sample.

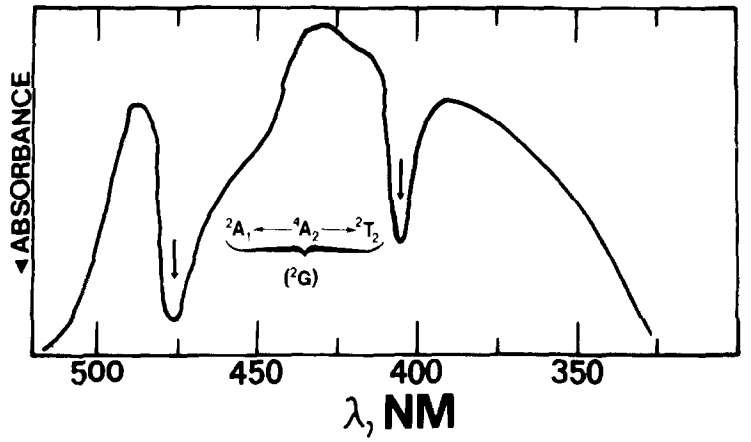

FIG. 5. Absorption spectrum at 77°K of 1 w/o Co-doped β-alumina; polycrystalline sintered material.

cobalt in tetrahedral coordination (*17–19*). The intensity of absorption is very large with an extinction coefficient of ca. 1100 (cm-mole/liter)$^{-1}$. The energies of the spin-forbidden transitions (Fig. 5) are also in agreement with the tetrahedral coordination for Co(II). the transition $^4T_1(^4F) \leftarrow {}^4A_2(^4F)$ could not be resolved. The infrared was investigated using KBr disks (*20*) for the $^4T_2(^4F) \leftarrow {}^4A_2(^4F)$ transition but it, too, could not be found. Because of the non-observance of another spin-allowed band, values for Dq and B could not be calculated. However, the crystal-field splitting of cobalt in β-alumina is approximately equal to that in the spinels $LiAl_5O_8$ and $ZnAl_2O_4$ (*21*) and somewhat greater than that in ZnO (*22*), judging from the position of the $^4T_1(^4P) \leftarrow {}^4A_2(^4F)$ transition.

No emission which could be attributed to cobalt was detected between 9000 and 25 000 cm^{-1}, the limits of the apparatus used for the emission spectroscopic investigation.

Magnetic Susceptibility

Figure 6 shows the temperature dependence of the susceptibility for cobalt in β-alumina. As expected, the susceptibility obeys the Langevin–Debye equation (*17*). The behavior of the magnetic moment is shown in Fig. 7 and is temperature independent. The moment calculated from the slope of Fig. 6 is 4.48 ± 0.07 μB. A Weiss temperature (Fig. 6) of -10 ± 2°K was found. A plot of χ_M vs $(T-\theta)^{-1}$ gives an estimate of TIP for this ion. TIP was found to be 0.6×10^{-3} erg/G^2 mole. These results are in excellent agreement with previous studies of tetrahedral cobalt (*22, 23*).

With the experimental estimate for TIP and the following relation for A_2 symmetry ground states (*17, 23*),

$$\chi_A^{TIP} = 8N\beta^2/10Dq,$$

where $N\beta^2 = 0.261$ cm^{-1}, we obtain $10Dq \cong 3500$ cm^{-1} which is reasonable for tetrahedral cobalt. This value of $10Dq$ gives a value for B (*24*) of 800 cm^{-1} which will place

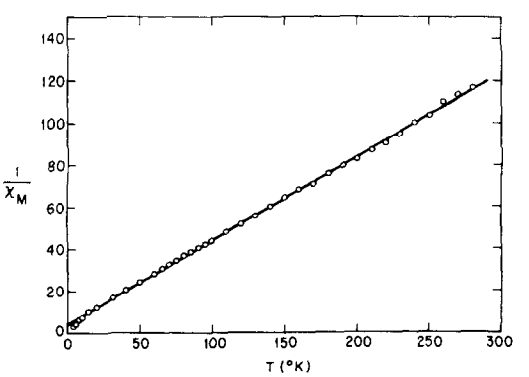

FIG. 6. Temperature dependence of the magnetic susceptibility for Co-doped β-alumina.

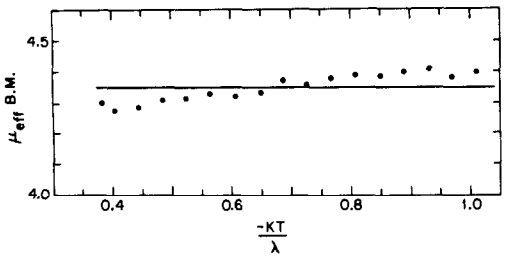

FIG. 7. Temperature dependence of the magnetic moment for Co-doped β-alumina.

the $^4T_1(^4P) \leftarrow {}^4A_2(^4F)$ transition at about the correct energy on the Tanabe–Sugano diagram. These calculations must be taken as approximate. They do indicate that the values reported by different techniques are consistent. At best the absolute value with which TIP is reported here is perhaps within 20% of the true value. It would be much more satisfying to obtain a direct measure of $10Dq$ from the $^4T_2(^4F) \leftarrow {}^4A_2(^4F)$ transition but that absorption has so far escaped detection.

In order to determine the TIP contribution to the total susceptibility more accurately it is necessary to investigate the behavior of the susceptibility at higher temperatures (*23*). At the highest temperature in this study (300°K), $\chi_M = 1.45 \times 10^{-2}$ erg/G^2 mole. TIP was therefore only about 5% of this value. This was too small a contribution to the total susceptibility for its effects to be noticeable in the χ_M^{-1} vs T plot of Fig. 6. At still higher temperatures TIP does become a larger contributor to the total susceptibility which results in the bending of the χ_M^{-1} vs T plot toward the temperature axis (*23*).

Nickel

Absorption Spectrum

Nickel occurs in spinels in both octahedral and tetrahedral coordination even though it is generally thought to prefer octahedral stereochemistry (*25, 26*). Figure 8 shows absorptions from both coordination sites except $^4T_{2g}(^4F) \leftarrow {}^4T_{1g}(^4F)$, which is not shown. The doublet nature of the $^3T_1(^3P) \leftarrow {}^3T_1(^3F)$ is due to the lifting of the degeneracy of the $^3T_1(^3P)$ term by the less-than-tetrahedral symmetry at the Ni(II) site

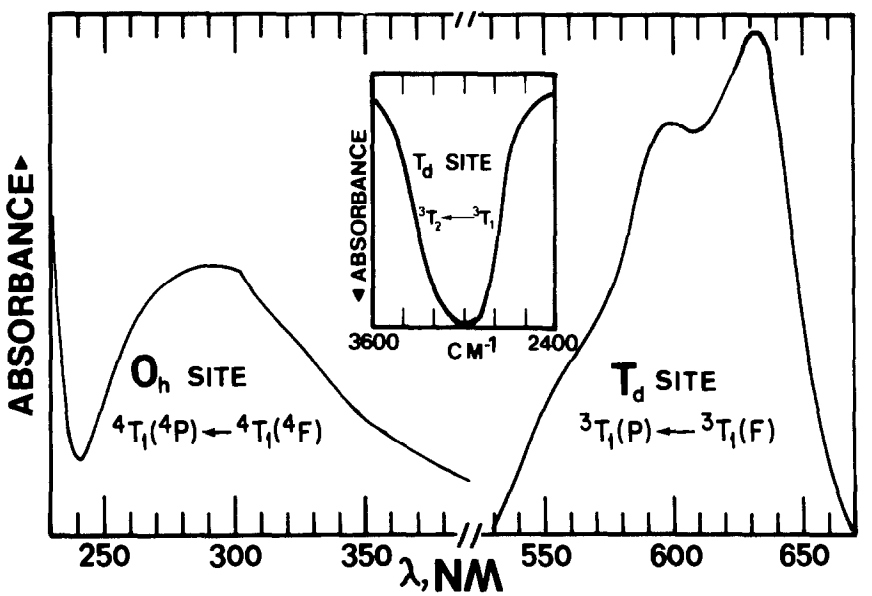

FIG. 8. Absorption spectrum at ambient temperature of 2 w/o Ni-doped β-alumina. One absorption not shown; see text.

(*17, 21*). The detection of the $^3T_2(^3F) \leftarrow {}^3T_1(^3F)$ in the ir enables the calculation of Dq and B for Ni(II) on tetrahedral sites. The results are contained in Table I. The values for Dq and B are in agreement with other reported values (*21, 27, 28*).

The absorptions at 290 nm (34 480 cm^{-1}; Fig. 8) and 490 nm (20 414 cm^{-1}; not shown in Fig. 8) were originally thought to be Ni(II) in octahedral symmetry. The absorptions are at such high energies, however, that they do not correlate with published values for Ni(II) in octahedral symmetry (*29–31*). Since it is known that Ni(III) can be prepared by heating NiO with alkali metal oxides in the presence of oxygen (*32*), and Ni(III) has been observed in other oxides (*33, 34*), it was hypothesized that the absorptions were due to Ni(III). Calculations for Dq and B were performed and the results are presented in Table I. The fit to the Tanabe–Sugano diagram for a d^7 high-spin octahedrally coordinated ion is quite satisfactory. The value of $10Dq/B = 21$ is near the value 22.5 whereby a low-spin complex would be expected. The absorption band positions rule out this possibility since the energy ratio of 34 480 cm^{-1}/20 414 cm^{-1} = 1.7 cannot be satisfactorily fit to the right side of the Tanabe–Sugano diagram for a d^7 ion regardless of the band assignment of the two observed transitions within the spin-allowed doublet levels.

The absorption peaks at 290 and 490 nm suggest that some of the nickel in β-alumina has been oxidized to Ni(III) and resides on octahedral sites in a high-spin state.

No emission from nickel-doped β-alumina was detected.

Magnetic Susceptibility

The ground state of tetrahedral Ni(II) is $^3T_1$ while that of octahedral Ni(III) is $^4T_1$. Both of these ground-state symmetries will be expected to give rise to magnetic behavior which does not follow the Langevin–Debye equation. Figure 9 shows the behavior of χ_g^{-1} vs T which deviates markedly from linearity especially at low temperatures. Since the nickel-doped specimen is probably a mixture of oxidation states whose exact ratios are unknown, values for χ_M cannot be calculated. It is sufficient to say that the susceptibility measurements are consistent with the absorption results that nickel additions to β-alumina may result in rather complex mixtures of oxidation states and site symmetry distributions.

Conclusion

The dopant metals Co(II) and Mn(II) are very stable in β-alumina. No changes in absorption spectra or magnetic susceptibilities (and emission spectrum for Mn) were noted upon changing from oxidizing to reducing firing atmospheres for the two metal dopants. The Mn(II) ion was the only species detectable even when MnO_2 was utilized as the dopant oxide and firing was in air. Manganese-doped β-alumina could not, however, be hot pressed in direct contact with graphite dies without reduction to the free metal which resulted in a black sample. Hot pressing in direct contact with graphite without reduction was possible for cobalt-doped β-alumina.

The results for nickel are interesting because of the apparent presence of Ni(III).

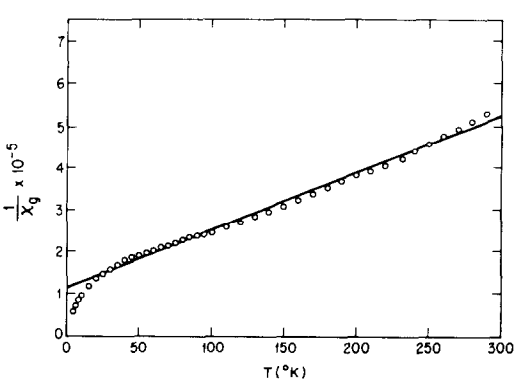

FIG. 9. Temperature dependence of the magnetic susceptibility for Ni-doped β-alumina.

The Ni(III) ion has been prepared previously but is still little studied. The unique high basicity coupled with a remarkable ability to absorb defects in its crystal structure make β-alumina a useful host lattice in which to produce unusual oxidation states in sufficient concentration for study.

In conclusion, a summary can now be presented for all the transition metal ions used in our studies to date (Table II).

Acknowledgment

The authors acknowledge partial financial support of this project by the National Science Foundation, Grants DMR 73-07507 A02 and DMR 77-24562. J.R.A. wishes to express his appreciation to Mr. R. Buder, Groupe des Transitions de Phase, CNRS, B.P. 166, 38042 Grenoble, France, for obtaining the magnetic susceptibility measurements. J.R.A. thanks the National Center for Scientific Research (CNRS) of France for an award under the United States–France Exchange of Scientists Program.

References

1. J. R. AKRIDGE, B. SROUR, C. MEYER, Y. GROS, AND J. H. KENNEDY, *J. Solid State Chem.* **25**, 169 (1978).
2. J. R. AKRIDGE AND J. H. KENNEDY, *J. Solid State Chem.* **26**, 147 (1978).
3. E. B. SANDELL, "Colorimetric Determination of Traces of Metals," 3rd ed., Interscience, New York (1959).
4. A. BERGSTEIN AND W. B. WHITE, *J. Inorg. Nucl. Chem.* **33**, 1629 (1971).
5. J. M. P. J. VERSTEGEN AND J. L. SOMMERDIJK, *J. Lumin.* **10**, 31 (1975).
6. R. C. BARKLIE AND K. O'DONNELL, *J. Phys. C* **10**, 4127 (1977).
7. R. C. BARKLIE, K. O'DONNELL, AND A. MURTAGH, *J. Phys. C* **10**, 4815 (1977).
8. Y. TANABE AND S. SUGANO, *J. Phys. Soc. Japan* **9**, 753 (1954).
9. D. T. PALUMBO AND J. J. BROWN, *J. Electrochem. Soc.* **117**, 1184 (1970).
10. C. R. PETERS, M. BETTMAN, J. W. MOORE, AND M. D. GLICK, *Acta Crystallogr. Sect. B* **27**, 1826 (1971).
11. D. T. PALUMBO AND J. J. BROWN, JR., *J. Electrochem. Soc.* **118**, 1159 (1971).
12. F. A. HUMMEL AND J. F. SARVER, *J. Electrochem. Soc.* **111**, 252 (1964).
13. P. M. JAFFE, *J. Electrochem. Soc.* **115**, 1203 (1968).
14. J. P. BOILOT, A. KAHN, J. THERY, R. COLLONGUES, J. ANTOINE, D. VIVIEN, C. CHEVRETTE, AND D. GOURIER, *Electrochim. Acta* **22**, 741 (1977).
15. J. ANTOINE, Ph.D. thesis, L'Université Pierre et Marie Curie, Paris 6 (October 22, 1976).
16. P. D. DERNIER AND J. P. REMEIKA, *J. Solid State Chem.* **17**, 245 (1976).

TABLE II

SUMMARY OF OXIDATION STATES AND SITES FOR TRANSITION METAL IONS IN β-ALUMINA

Metal	Firing atmosphere	Oxidation states	Site in alumina
Fe	Air	+2	Tetrahedral; Al(2) most likely
		+3	Tetrahedral; could be Al(2) or Al(3) or distribution over both sites
	H_2/N_2	+2	Tetrahedral
Cr	Air	+4	Octahedral; Al(1)[a]
	H_2/N_2	+3	Octahedral; Al(1)[a]
Co	Air	+2	Tetrahedral; Al(2)[b]
	H_2/N_2	+2	Tetrahedral; Al(2)[b]
Mn	Air	+2	Tetrahedral; Al(2)[a]
	H_2/N_2	+2	Tetrahedral; Al(2)[a]
Ni	Air	+2	Tetrahedral; Al(2) most likely
		+3	Octahedral; Al(1) most likely
	H_2/N_2	0	Unknown

[a] See Ref. (*14*).
[b] See Ref. (*16*).

17. B. N. FIGGIS, "Introduction to Ligand Fields," p. 241, Ch. 10, Interscience, New York (1966).
18. A. B. P. LEVER, "Inorganic Electronic Spectroscopy," pp. 322–325, Elsevier, Amsterdam/New York (1968).
19. F. A. COTTON, D. M. L. GOODGAME, AND M. GOODGAME, *J. Amer. Chem. Soc.* **83**, 4690 (1961).
20. L. F. POWER AND A. M. TAIT, *Anal. Chem.* **47**, 1721 (1975).
21. R. D. GILLEN AND R. E. SOLOMON, *J. Phys. Chem.* **74**, 4252 (1970).
22. F. PEPE, M. SCHIAVELLO, AND G. FERRARIS, *J. Solid State Chem.* **12**, 63 (1975).
23. P. COSSEE AND A. E. VAN ARKEL, *J. Phys. Chem. Solids* **15**, 1 (1960).
24. A. B. P. LEVER, "Inorganic Electronic Spectroscopy," pp. 182–183, Elsevier, Amsterdam/New York (1968).
25. A. MILLER, *J. Applied Phys. Suppl.* **30**, 245 (1959).
26. G. BLASSE, *Progr. Ceram. Sci.* **4**, 133 (1966).
27. F. A. COTTON AND G. WILKINSON, "Advanced Inorganic Chemistry," 3rd ed., pp. 894 and 896, Interscience, New York (1972).
28. M. I. BÁN, J. CSÁSZÁR, AND M. HEGYHÁTI, *J. Mol. Struct.* **19**, 455 (1973).
29. R. NEWMAN AND R. M. CHRENKO, *Phys. Rev.* **114**, 1507 (1959).
30. P. BRINT, A. J. MCCAFFERY, R. GALE, AND M. D. ROWE, *Inorg. Chem.* **11**, 2627 (1972).
31. W. LOW, *Phys. Rev.* **109**, 247 (1958).
32. F. A. COTTON AND G. WILKINSON, "Advanced Inorganic Chemistry," 3rd ed., p. 901, Interscience, New York (1972).
33. M. ARJOMAND AND D. J. MACHIN, *J. Chem. Soc. Dalton*, 1055 (1975).
34. K. W. BLAZEY, P. KOIDL, W. BERLINGER, AND K. A. MÜLLER, *Ferroelectrics* **13**, 289 (1976).